Climate and human influences on global biomass burning over the past two millennia

J. R. MARLON[1]*, P. J. BARTLEIN[1], C. CARCAILLET[2], D. G. GAVIN[1], S. P. HARRISON[3], P. E. HIGUERA[4], F. JOOS[5], M. J. POWER[6] AND I. C. PRENTICE[7]

[1]Department of Geography, University of Oregon, Eugene, Oregon 97403, USA
[2]Centre for Bio-Archaeology and Ecology (UMR5059 CNRS/UM2/EPHE), Institut de Botanique, F-34090 Montpellier, France
[3]School of Geographical Sciences, University of Bristol, Bristol BS8 1SS, UK
[4]Department of Earth Sciences, Montana State University, Bozeman, Montana 59717, USA
[5]Climate and Environmental Physics, Physics Institute and Oeschger Centre for Climate Change Research, University of Bern, CH-3012 Bern, Switzerland
[6]Utah Museum of Natural History, Department of Geography, University of Utah, Salt Lake City, Utah 84112, USA
[7]QUEST, Department of Earth Sciences, University of Bristol, Bristol BS8 1RJ, UK
*e-mail: jmarlon@uoregon.edu

Published online: 21 September 2008; doi:10.1038/ngeo313

Large, well-documented wildfires have recently generated worldwide attention, and raised concerns about the impacts of humans and climate change on wildfire regimes. However, comparatively little is known about the patterns and driving forces of global fire activity before the twentieth century. Here we compile sedimentary charcoal records spanning six continents to document trends in both natural and anthropogenic biomass burning for the past two millennia. We find that global biomass burning declined from AD 1 to ~1750, before rising sharply between 1750 and 1870. Global burning then declined abruptly after 1870. The early decline in biomass burning occurred in concert with a global cooling trend and despite a rise in the human population. We suggest the subsequent rise was linked to increasing human influences, such as population growth and land-use changes. Our compilation suggests that the final decline occurred despite increasing air temperatures and population. We attribute this reduction in the amount of biomass burned over the past 150 years to the global expansion of intensive grazing, agriculture and fire management.

Fire is a key Earth system process affecting ecosystems, land-surface properties, the carbon cycle, atmospheric chemistry, aerosols and human activities. Humans manage fire intensively today, so it is easy to forget that fire is a natural process that has dominated the ecology of many terrestrial ecosystems throughout their history[1–3]. Empirical data on long-term changes in fire activity, particularly at broad spatial scales, however, are limited. Historical records[4], remotely sensed data[5] and tree-ring data from the past few centuries[6–8] provide most of the information about the interactions of fire, climate, vegetation and people. Climate-change projections indicate that we will be moving quickly out of the range of the natural variability of the past few centuries. Charcoal records from lake sediments enable us to infer the impacts of climate changes and human activities on global biomass burning during periods when both have changed substantially. Although hundreds of such records have been developed during palaeoecological analyses[9,10], until now no attempt has been made to analyse them for large-scale patterns and trends over the past 2,000 years.

We present global and regional reconstructions of biomass burned over the past 2,000 years (Figs 1 and 2) based on a global sedimentary charcoal data set (Fig. 3). We interpret temporal patterns in biomass burned, as indicated by changes in the input of charcoal to sediments, by comparison with independent reconstructions of human population and temperature changes, and with climate simulations that mimic the broad features of reconstructed temperature changes.

CHARCOAL RECORDS OF BIOMASS BURNING

Charcoal accumulation in sediments has been shown[11,12] to reflect biomass burning within tens of kilometres of the sampling site. We developed regional and global composite stratigraphies based on 406 charcoal records from lake sediments and peats. Although there are geographic gaps, there is good coverage of climatic zones and of all the major biomes except grassland/dry shrubland (Fig. 3; Supplementary Information, Fig. S1), where low woody biomass limits charcoal production. Composite records were standardized and transformed (see Supplementary Information) to represent centennial-scale trends in charcoal accumulation rates or 'influx' (in units of quantity area^{-1} yr^{-1}) for the globe or a given region and to reveal the relative changes in biomass burned through time[11]. Interannual to decadal variations are not resolved, so these data do not record changes that might be attributable to higher-frequency climate variability or land management changes over the past few decades[5,6]. The strength of these data lies in their ability to provide a long-term observational record with site coverage that does not degrade substantially with increasing time from the present.

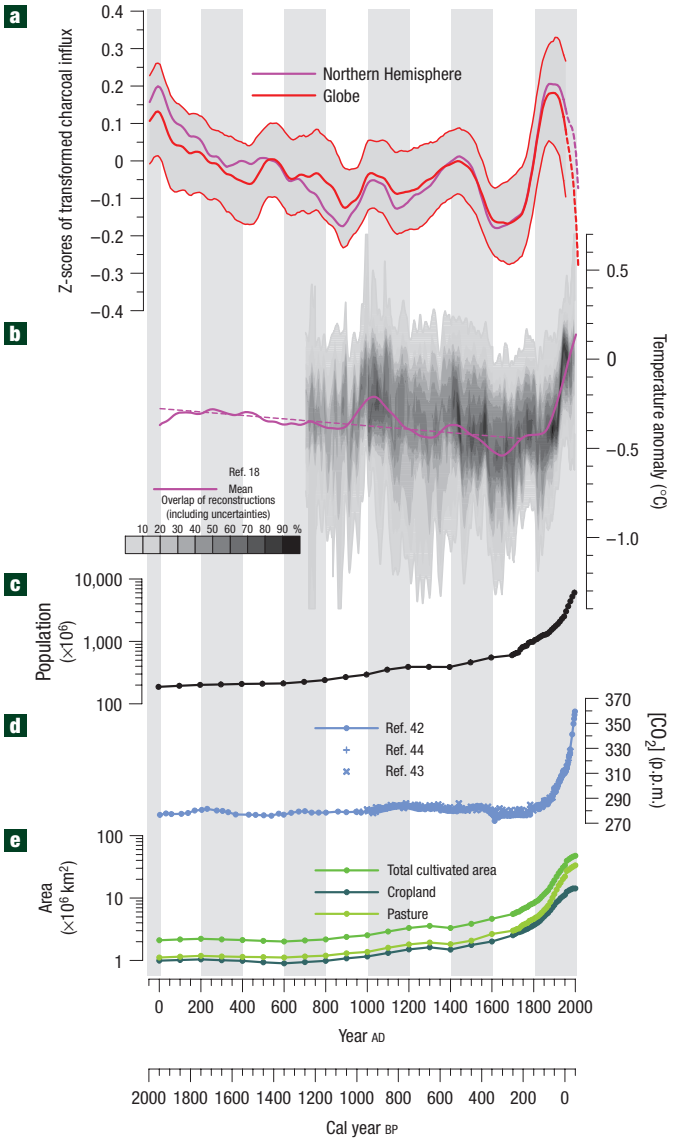

Figure 1 Reconstructions of biomass burning, climate, population and land cover. a, Reconstruction of global (red line) and Northern Hemisphere (purple line) biomass burning with confidence intervals based on bootstrap resampling by site. A dashed line is used to represent increased uncertainty in late twentieth century changes in biomass burning. **b**, Reconstructions of Northern Hemisphere climate[18] with mean values (purple line) of available reconstructions, trend line (dotted line) for first part of record and overlap of uncertainty ranges of ten Northern Hemisphere temperature reconstructions after AD 700 (grey shading). **c**, World population from the HYDE 3.0 database[30]. **d**, Atmospheric CO_2 concentration[42–44]. **e**, Global agricultural land cover[30].

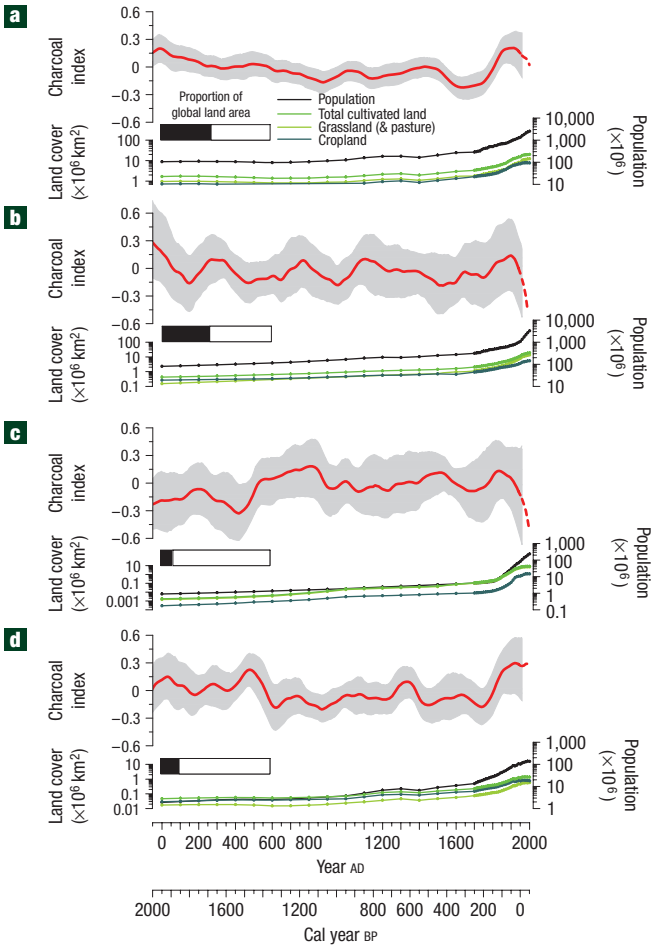

Figure 2 Zonal changes in biomass burning, population and land cover. a–d, Changes in biomass burning (as in Fig. 1) with land-cover change[30], and proportion of global ice-free land area, for northern extratropics (>30° N) (**a**), tropics (30° N to 20° S) (**b**), southern extratropics (>20° S) (**c**) and the northern high latitudes (>55° N) (**d**). The composite records are based on at least 10 sites per region and thus should reveal the dominant patterns that reflect processes operating at large spatial scales (see Methods section).

The global sedimentary charcoal record (Fig. 1a) shows a long-term decline in biomass burning from AD 1 to about 1750, followed by a marked increase. A maximum, corresponding to the highest biomass-burning rate in the past two millennia, occurs around AD 1870. This maximum is followed by a sharp downturn in the composite record. At centennial scales, there is a local maximum in biomass burning at AD 1 that does not correspond to warmer temperatures, but the temperature reconstruction consists of only two records during this period. Biomass-burning minima occur about AD 400 and 900, and at 1700, during the 'Little Ice Age' (about 1400–1800). Our analyses (see Supplementary Information) show that these patterns in the global record are robust and unaffected by differences in record type or sampling resolution, changes in sedimentation rates and age model construction, or by the choice of statistical techniques used to construct the composite records.

The long-term decline in biomass burning before 1750 is most strongly expressed in the northern extratropics (Fig. 2), particularly in western North America and Asia (see Supplementary Information, Figs S11,S14). The long-term decline is also characteristic of records from Central and tropical South America (Fig. 4), although the decrease in biomass burning there occurs earlier (~1300) and persists longer than in other regions. In contrast, the tropics and southern extratropics show variable levels of biomass burning to ~1850, after which the records show a widespread decline in biomass burning (see Supplementary Information, Figs S8,S9).

Increased burning in the tropics and western United States during the past three decades has been widely reported[5,6,13,14]. The

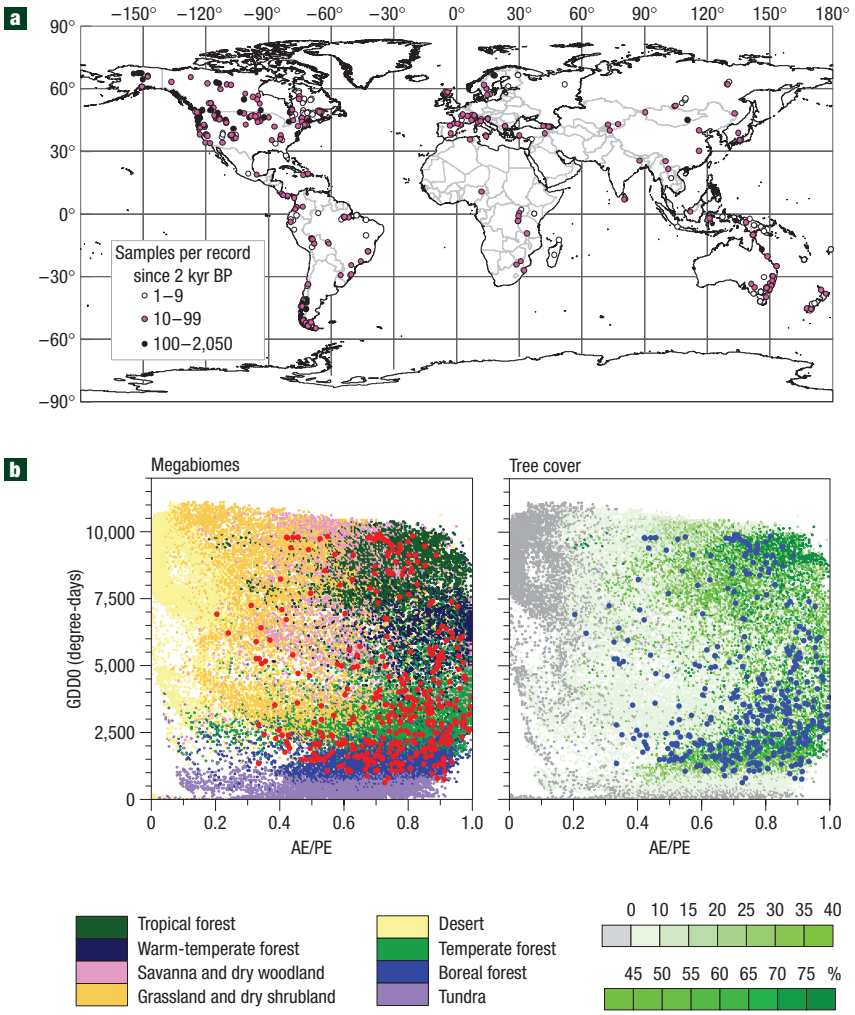

Figure 3 Distribution of sites in geographic, climate and vegetation space. a, Locations of charcoal records and number of samples over the past 2,000 years (see Methods section). Mean sampling density is one sample per 70 years. **b**, Distribution of records in bioclimate space showing locations plotted against growing degree-days above 0 °C (an index of effective warmth during the growing season) and the ratio of actual to equilibrium evapotranspiration (an index of effective moisture)[45,46], with remotely sensed tree cover[47] and modelled biome[48] shown for comparison.

global charcoal record does not reflect this for a variety of reasons, including data coverage, methodological issues and chronological constraints in core-top sediments. For example, many of the charcoal records from the tropics do not span the most recent few decades. In addition, the geographic coverage of lakes and bogs in the tropics does not overlap well with the areas of most severe burning (Fig. 3). However, individual palaeofire records near areas of recent severe burning do show increasing charcoal levels towards present. For example, the only site in Kalimantan[15], Indonesia, where extensive peat fires occurred, indicates high biomass burning in the past few decades. This is true in the western United States as well[16,17]. Additional data and regional syntheses are needed to resolve these patterns.

CLIMATE, POPULATION AND BIOMASS BURNING

Comparisons of global biomass burning with reconstructed and simulated climate conditions during the past two millennia show strong similarities until the Industrial Revolution, ~1750 (Fig. 1b, Supplementary Information, Fig. S5). Reconstructions of Northern Hemisphere mean annual temperature from palaeoclimatic evidence[18] show a gradual cooling trend from 1 AD to 1750. Simulated temperatures show a similar decline[19] (see Supplementary Information, Fig. S5). Global and Northern Hemisphere reconstructed temperatures show local maxima around 1000 and 1400, corresponding to the local maxima in charcoal influx, and a pronounced decline from 1400 to 1700 (Fig. 1b).

Over the interval from 1 to 1750, world population and land-cover conversion to agriculture generally increased (Fig. 1c,e) with a very slight century-scale decrease related to the Black Death in Europe (about 1300 to 1400). Population growth and accompanying land-cover change therefore do not account for the apparent decrease in global biomass burning during the first phase of the composite record. Conversely, the correspondence between declining biomass burning and long-term cooling on hemispheric or global scales can be explained by the positive temperature dependence of fuel moisture (and hence flammability) and vegetation productivity (and hence fuel availability) in cooler climates.

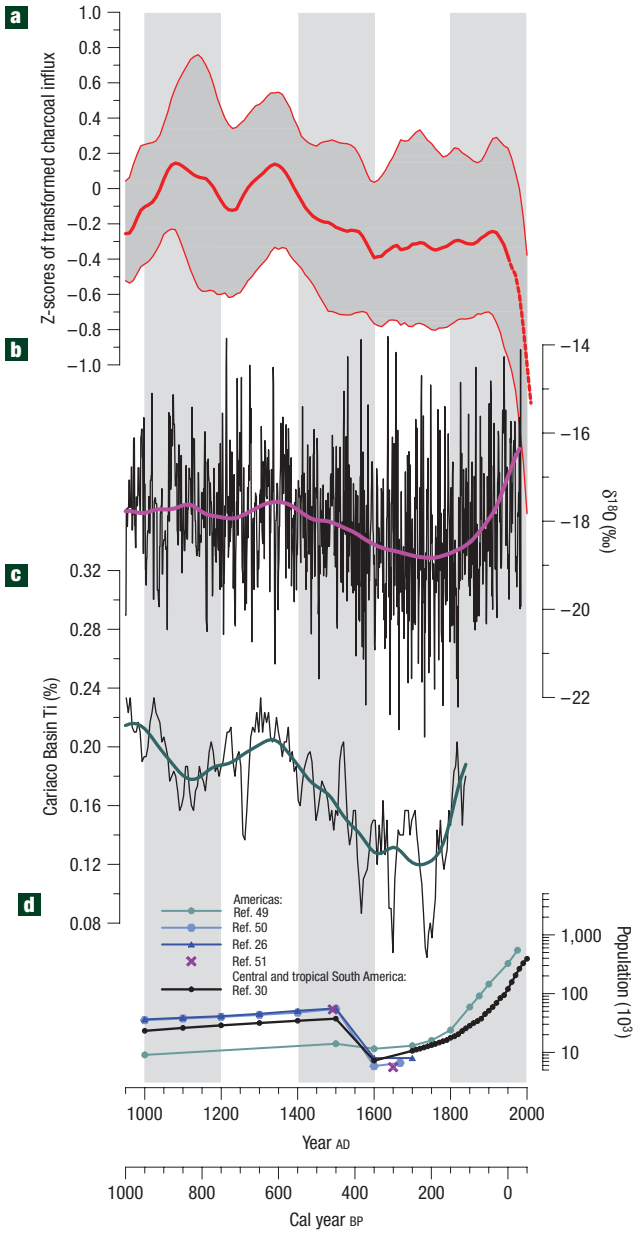

Figure 4 Comparison of biomass-burning reconstruction for Central and tropical South America with climate and population data. a–c, Biomass-burning reconstruction for Central and tropical South America (20° S to 30° N) for the past 1,000 years (**a**), with oxygen isotope data from the Quelccaya ice core[31] (**b**) and titanium concentration from a Cariaco Basin marine core[32] (**c**), both smoothed as the charcoal records. **d**, Population estimates for the Americas[30] derived from archaeological records[26,27,30,49,50]. The two crosses are estimates of the population of the Americas before and after European contact from ref. 51.

Biomass burning sharply increased around 1750; temperatures (Fig. 1b, Supplementary Information, Fig. S5), greenhouse-gas concentrations (Fig. 1d) and the rates of land-cover conversion and population growth (Fig. 1c,e) also began to increase. Increasing temperatures, rapidly increasing population and land-cover conversion and rising CO_2 (promoting an increase in biomass through CO_2 fertilization) could in principle all have contributed to the biomass-burning increase. However, after ~1870, a sharp downturn in biomass burning occurs despite accelerated increases in temperature and CO_2, strongly suggesting the involvement of human activity. The decades following 1870 coincide with the period of maximum expansion of population and agriculture (Figs 1c,e, and 2), so the biomass-burning decrease beginning then certainly cannot be explained by reduced human activity. Indeed, this has been the period of most rapid land-use change, characterized by large-scale conversion of native vegetation to croplands and the widespread introduction of domestic grazing animals such as cows and sheep[20–22]. We therefore suggest that the downturn can plausibly be explained as an effect of land-use change, resulting in landscape fragmentation and a generally less flammable landscape in many regions[23]. Active fire suppression since the early twentieth century has also presumably reduced total biomass burning in recent decades.

Records from the northern high-latitude regions (poleward of 55° N) show the general climate-induced decline and the post-1750 increase in biomass burning characteristic of the global signal but do not show the recent downturn in biomass burning (Fig. 2d, Supplementary Information, Fig. S10). This region has been much less affected by agricultural expansion than regions farther south (Fig. 2), and is influenced by high-latitude amplification of the global-warming signal leading to increased temperatures, dryness and greater fire activity[24,25]. The biomass-burning record from Europe (see Supplementary Information, Fig. S13), which has been subject to agricultural exploitation throughout the past two millennia, also fails to show the recent downturn, consistent with our explanation. The regions in which the downturn is most strongly expressed, including western North America (see Supplementary Information, Fig. S11), the tropics (Fig. 2b and Supplementary Information, Fig. S8) and Asia (see Supplementary Information, Fig. S14), are characterized by strong intensification of land management since the mid-nineteenth century. Although initial colonization may have been marked by an increased use of fire for land clearance, the expansion of intensive agriculture and forest management activities in these regions was associated with a reduced incidence of fire[23].

The record of global biomass burning over the past 2,000 years can be divided into four distinct intervals: (1) 1–1750, when climate drove the long-term downward trend in biomass burning; (2) 1750 to late nineteenth century, when population-driven land-cover changes along with increases in global temperatures produced the sharp increase in biomass burning, (3) late nineteenth to mid-to-late twentieth century, which includes the striking decrease in biomass burning that accompanies the decrease in the rate of land-cover change; and (4) the past several decades, which is beyond the resolving power of the global charcoal record, when increased biomass burning is reported in many tropical regions.

FIRE AND ATMOSPHERIC CHEMISTRY

Ferretti *et al.*[26] showed an 'unexpected' trend towards more negative $\delta^{13}CH_4$ values from AD 1 to 1700 in the Law Dome ice-core record, and invoked changes in biomass burning to explain this trend. They noted the similarity of their $\delta^{13}CH_4$ record both to the Law Dome record of atmospheric CO concentration and to proxy-based reconstructions of Northern Hemisphere temperatures. Because fire is a major source of CO and the main natural source of relatively ^{13}C-enriched CH_4, Ferretti *et al.* postulated a declining trend in biomass burning, and attributed it to long-term cooling of the land surface. Houweling *et al.*[27] expressed scepticism about this possibility and proposed an alternative scenario involving changing wetland emissions, plant emissions and early rice cultivation to explain the $\delta^{13}CH_4$ trend, avoiding the implication of Ferretti *et al.* of high biomass-burning levels in pre-industrial time. Our results

however provide strong empirical support for the decline in biomass burning since 1 AD proposed by Ferretti *et al.*[26].

Ferretti *et al.* also noted an especially steep fall in $\delta^{13}CH_4$ from 1500 to 1700, and invoked population decline in the Americas as an extra factor to account for it. The global charcoal record also shows a sharp decrease from 1500 to 1700, but global population did not fall during this period (Fig. 1c). South American population declined after 1500 (refs 28,29) (Fig. 4), but a comparison of biomass burning, population estimates for the Americas[30] and climate data from Andean ice cores[31] and Cariaco Basin titanium concentrations[32], which is a proxy for Atlantic Intertropical Convergence Zone latitude and hence tropical precipitation trends, suggests that the largest decrease in biomass burning there preceded the population decline and followed regional climate trends (Fig. 4). The similarities between the global charcoal record and climate proxies suggest a continuing climatic control to at least 1750.

The peak in global biomass burning at ~1870 corresponds to a peak in black carbon around 1900 observed in Greenland ice; however, McConnell *et al.*[33] attribute this to a peak in industrial emissions. The separation of biomass and fossil components of the black-carbon record, however, rests on the interpretation of the accompanying vanillic acid record as a proxy for global biomass burning[34] and, in part, on the choice of scaling factors between vanillic acid and black carbon.

Our results strongly suggest that climate change has been the main driver of global biomass burning for the past two millennia. The decline in biomass burning after 1870 is opposite to the expected effect of rising CO_2 and rapid warming, but contemporaneous with an unprecedentedly high rate of population increase. This suggests that, during the industrial era, a major impact of human activities has been to reduce biomass burning through the large-scale expansion of intensive grazing and cropping with associated landscape fragmentation, and also active fire management. However, in regions less dominated by intensive land management, wildland fire has remained at high levels or increased as the climate has warmed. In the future, it is plausible that the main impact of human activity on burning will be through anthropogenic climate change[35]. To assess this possibility, it will be necessary to improve our understanding of palaeoecological records of fire and to develop reliable models of the fire regime. Such models should include human as well as natural ignitions, account for the effects of land use as well as climate and be tested using palaeoecological and ice-core data[36].

METHODS

Analyses are based on 406 sedimentary charcoal records from the Global Charcoal Database (GCD version 1) (ref. 10), plus supplementary data from members of the Global Palaeofire Working Group that will be incorporated into GCD version 2. Only records from lakes, bogs and small hollows were included in our analyses (see Supplementary Information).

We examined the distribution of data in terms of geographic, climatic and vegetation space to ensure that the data set could be considered a reasonable representation of global biomass burning. Given the unequal distribution of land between the Northern and Southern hemispheres, the charcoal data set is reasonably representative of the globe. Sixty-seven per cent of the sites are in the Northern Hemisphere, which represents ~74% of the ice-free land area. Nevertheless, some geographic regions are less well sampled than others (Fig. 3). To assess the global coverage of the GCD in terms of climate and vegetation, we plotted individual charcoal sites on top of climate, simulated biomes and tree cover data (Fig. 3). The charcoal sites provide a reasonably representative sampling of all the major climatic zones, and of forest biomes (see Supplementary Information, Fig. S1). Grassland/dry shrubland, savannas and deserts are under-represented (Fig. 3). There are few natural fires in desert regions; thus, this under-sampling is not important. The paucity of charcoal records from grassland and dry shrubland and from savanna reflects the dominance of low-intensity ground fires in these regions and the smaller number of lakes present in dry regions. Such low-intensity fires do not consistently leave a charcoal record (although see ref. 37), and the total biomass burned is low compared with forests[38]. Thus, the under-sampling of these two vegetation types is unlikely to affect the composite global biomass-burning curve significantly.

The broad range of data types and charcoal quantification methods, as well as the skewed distribution of most charcoal records, motivated the transformation and standardization of the data before generating composite records. After testing the impact of several standardization and normalization techniques, we chose to use a modified version (see Supplementary Information) of the normalization and standardization procedure described by Power *et al.*[10], which resulted in highly robust charcoal summarizations.

Charcoal data were normalized to stabilize the variance and standardized to make them comparable across a broad range of data types, sampling and processing methods. Records were smoothed by fitting lowess curves[39] to the data in a two-stage process that prevented records with the highest resolution from dominating the global signal, and that avoided interpolating data in the low-resolution records. This approach also minimizes the impact of the extreme values in sedimentary charcoal data, which enabled us to focus instead on the long-term trends in the data. Various sensitivity analyses were carried out to ensure that the composite records were robust to the use of influx versus concentration values, to the effects of changing sedimentation rates and to the differences in coverage among regions (see Supplementary Information).

We compared the reconstructed changes in fire regimes with climate proxy records of Northern Hemisphere temperature variations during the past 2,000 years[18], and confirmed that these data series are statistically correlated during the interval from 1 to 1750 AD (see Supplementary Information). We used ten Northern Hemisphere temperature reconstructions based on multiple climate proxies. These reconstructions differ in (1) data type, (2) data origin (terrestrial and/or marine), (3) inclusion or exclusion of extratropical data sources, (4) the number of data points used in the final reconstructions, (5) temporal length, (6) seasonal specificity (summer versus mean annual temperature) and (7) statistical methods used to derive the reconstruction. Nevertheless, as shown in the Intergovernmental Panel on Climate Change Fourth Assessment[18], the reconstructions show broad coherence over the past 1,300 years on centennial timescales, and the existence of multiple reconstructions makes it possible to derive confidence limits based on the degree of coherence between the available reconstructions. Here we use the mean of the ten available reconstructions, smoothed with a lowess curve. We also show the uncertainties in the reconstructions.

There have been some attempts to reconstruct historical changes in global mean temperatures[40], and in Southern Hemisphere temperatures[41]. Given the paucity of data available from the Southern Hemisphere covering more than the past few decades, comparison of such data with the reconstructed fire histories is unwarranted. However, we did compare simulated global changes in warm-season temperatures and dry-season precipitation rates from the National Center for Atmospheric Research Climate System Model (see Supplementary Information, Fig. S5).

To explain the variations in global biomass burning, we also compared the charcoal data with population and land-cover data. World population and land-cover data were obtained from the HYDE 3.0 database[30] and were summarized using lowess curves in a manner similar to the charcoal and climate data. Confidence intervals (95%) are also shown (Fig. 1).

Received 19 June 2008; accepted 27 August 2008; published 21 September 2008.

References

1. Scott, A. C. The pre-quaternary history of fire. *Palaeogeogr. Palaeoclimatol. Palaeoecol.* **164**, 281–329 (2000).
2. Bond, W. J. & Keeley, J. E. Fire as a global 'herbivore': The ecology and evolution of flammable ecosystems. *Trends Ecol. Evol.* **20**, 387–394 (2005).
3. Scott, A. C. & Glasspool, I. J. The diversification of Paleozoic fire systems and fluctuations in atmospheric oxygen concentration. *Proc. Natl Acad. Sci. USA* **103**, 10861–10865 (2006).
4. Westerling, A. L., Hidalgo, H. G., Cayan, D. R. & Swetnam, T. W. Warming and earlier spring increase western US forest wildfire activity. *Science* **313**, 940–943 (2006).
5. Van der Werf, G. R., Randerson, J. T., Giglio, L., Collatz, G. J. & Kasibhatla, P. S. Interannual variability in global biomass burning emission from 1997 to 2004. *Atmos. Chem. Phys.* **6**, 3423–3441 (2006).
6. Mouillot, F. & Field, C. B. Fire history and the global carbon budget: a 1° × 1° fire history reconstruction for the 20th century. *Glob. Change Biol.* **11**, 398–420 (2005).
7. Swetnam, T. W. & Betancourt, J. L. Mesoscale disturbance and ecological response to decadal climatic variability in the American southwest. *J. Clim.* **11**, 3128–3147 (1998).
8. Girardin, M. P. & Sauchyn, D. Three centuries of annual area burned variability in northwestern North America inferred from tree rings. *Holocene* **18**, 205–214 (2008).
9. Carcaillet, C. *et al.* Holocene biomass burning and global dynamics of the carbon cycle. *Chemosphere* **49**, 845–863 (2002).

10. Power, M. J. *et al.* Changes in fire regimes since the Last Glacial Maximum: An assessment based on a global synthesis and analysis of charcoal data. *Clim. Dyn.* **30**, 887–907 (2008).
11. Marlon, J., Bartlein, P. J. & Whitlock, C. Fire-fuel-climate linkages in the northwestern USA during the Holocene. *Holocene* **16**, 1059–1071 (2006).
12. Higuera, P. E., Peters, M. E., Brubaker, L. B. & Gavin, D. G. Understanding the origin and analysis of sediment-charcoal records with a simulation model. *Quat. Sci. Rev.* **26**, 1790–1809 (2007).
13. Page, S. E. *et al.* The amount of carbon released from peat and forest fires in Indonesia during 1997. *Nature* **420**, 61–65 (1997).
14. Cochrane, M. A. Fire science for rain forests. *Nature* **421**, 913–919 (2003).
15. Anshari, G., Peter Kershaw, A. & van der Kaars, S. A Late Pleistocene and Holocene pollen and charcoal record from peat swamp forest, Lake Sentarum Wildlife Reserve, West Kalimantan, Indonesia. *Palaeogeogr. Palaeoclimatol. Palaeoecol.* **171**, 213–228 (2001).
16. Millspaugh, S. H., Whitlock, C. & Bartlein, P. J. Variations in fire frequency and climate over the past 17000 yr in central Yellowstone National Park. *Geology* **28**, 211–214 (2000).
17. Millspaugh, S. H., Whitlock, C. & Bartlein, P. in *After the Fires: The Ecology of Change in Yellowstone National Park* (ed. Wallace, L.) 10–28 (Yale Univ. Press, New Haven, 2004).
18. Jansen, E. *et al.* in *Climate Change 2007: The Physical Science Basis. Contribution of Working Group I to the Fourth Assessment Report of the Intergovernmental Panel on Climate Change* (eds Solomon, S. *et al.*) 433–497 (Cambridge Univ. Press, Cambridge, 2007).
19. Ammann, C. M., Joos, F., Schimel, D. S., Otto-Bliesner, B. L. & Tomas, R. A. Solar influence on climate during the past millennium: Results from transient simulations with the NCAR Climate System Model. *Proc. Natl Acad. Sci. USA* **104**, 3713–3718 (2007).
20. Klein Goldewijk, K. & Ramankutty, N. Land cover change over the last three centuries due to human activities: The availability of new global data sets. *Geojournal* **61**, 335–344 (2004).
21. Savage, M. & Swetnam, T. W. Early 19th-century fire decline following sheep pasturing in a Navajo ponderosa pine forest. *Ecology* **71**, 2374–2378 (1990).
22. Swetnam, T. W. & Baisan, C. H. in *Fire and Climate in Temperate Ecosystems of the Western Americas* (eds Veblen, T. T., Baker, W. L., Montenegro, G. & Swetnam, T. W.) 158–195 (Springer, New York, 2003).
23. Pyne, S. J. *World Fire: The Culture of Fire on Earth* (Univ. of Washington Press, Seattle, 1995).
24. Chapin, F. S. III. *et al.* Role of land-surface changes in Arctic summer warming. *Science* **310**, 657–660 (2005).
25. Girardin, M. P. Interannual to decadal changes in area burned in Canada from 1781 to 1982 and the relationship to Northern Hemisphere land temperatures. *Glob. Ecol. Biogeog.* **16**, 557–566 (2007).
26. Ferretti, D. F. *et al.* Unexpected changes to the global methane budget over the past 2000 years. *Science* **309**, 1714–1717 (2005).
27. Houweling, S., van der Werf, G, Klein Goldewijk, K., Röckmann, T. & Aben, I. Early anthropogenic emissions and the variation of CH_4 and $^{13}CH_4$ over the last millennium. *Glob. Biogeochem. Cycles* **22**, GB1002doi:10.1029/2007GB002961 (2008).
28. Denevan, W. N. *The Native Population of Amazonia in 1492 Reconsidered* (2003).
29. Bush, M. B., Silman, M. R., McMichael, C. & Saatchi, S. Fire, climate change and biodiversity in Amazonia: A Late-Holocene perspective. *Phil. Trans. R. Soc. B* **363**, 1795–1802 (2008).
30. Klein Goldewijk, K. & van Drecht, G. in *Integrated Modelling of Global Environmental Change. An Overview of IMAGE 2.4* (eds Bouwman, A. F., Kram, T. & Klein Goldewijk, K.) (Netherlands Environmental Assessment Agency, Bilthoven, The Netherlands, 2006).
31. Thompson, L. G. *et al.* Tropical glacier and ice core evidence of climate change on annual to millennial time scales. *Clim. Change* **59**, 137–155 (2003).
32. Haug, G. H., Hughen, K. A., Sigman, D. M., Peterson, L. C. & Rohl, U. Southward migration of the intertropical convergence zone through the Holocene. *Science* **293**, 1304–1308 (2001).
33. McConnell, J. R. *et al.* 20th-century industrial black carbon emissions altered Arctic climate forcing. *Science* **317**, 1381–1384 (2007).
34. Oros, D. R. & Simoneit, B. R. T. Identification and emission factors of molecular tracers in organic aerosols from biomass burning Part 1. Temperate climate conifers. *Appl. Geochem.* **16**, 1513–1544 (2001).
35. Scholze, M., Knorr, W., Arneill, N. W. & Prentice, I. C. A climate-change risk analysis for world ecosystems. *Proc. Natl Acad. Sci. USA* **103**, 13116 (2006).
36. Running, S. W. Ecosystem disturbance, carbon, and climate. *Science* **321**, 652–653 (2008).
37. Wooller, M. J., Street-Perrott, F. A. & Agnew, A. D. Q. Late Quaternary fires and grassland palaeoecology of Mount Kenya, East Africa: Evidence from charred grass cuticles in lake sediments. *Palaeogeogr. Palaeoclimatol. Palaeoecol.* **164**, 207–230 (2000).
38. Stocks, B. J. & Kauffman, J. B. in *Sediment Records of Biomass Burning and Global Change* (eds Clark, J. S., Chachier, H., Goldammer, J. G. & Stocks, B.) 169–188 (Springer, Berlin, 1997).
39. Cleveland, W. S. & Devlin, S. J. Locally weighted regression: An approach to regression analysis by local fitting. *J. Am. Stat. Assoc.* **83**, 596–610 (1988).
40. Oerlemans, J. Extracting a climate signal from 169 glacier records. *Science* **308**, 675–677 (2005).
41. Mann, M. & Jones, P. Global surface temperatures over the past two millennia. *Geophys. Res. Lett.* **30**, 1820–1823 (2003).
42. Meure, C. M. *et al.* Law Dome CO_2, CH_4 and N_2O ice core records extended to 2000 years BP. *Geophys. Res. Lett.* **33**, L14810 (2006).
43. Siegenthaler, U. *et al.* Supporting evidence from the EPICA Dronning Maud Land ice core for atmospheric CO_2 changes during the past millennium. *Tellus: Series B* **57**, 51–57 (2005).
44. Etheridge, D. M. *et al.* Natural and anthropogenic changes in atmospheric CO_2 over the last 1000 years from air in Antarctic ice and firn. *J. Geophys. Res.* **101**, 4115–4128 (1996).
45. Prentice, I. C., Sykes, M. T. & Cramer, W. A simulation model for the transient effects of climate change on forest landscapes. *Ecol. Mod.* **65**, 51–70 (1993).
46. Shafer, S. L., Bartlein, P. J. & Thompson, R. S. Potential changes in the distributions of Western North America tree and shrub taxa under future climate scenarios. *Ecosystems* **4**, 200–215 (2001).
47. DeFries, R., Hansen, M., Townshend, J. R. G., Janetos, A. C. & Loveland, T. R. A new global 1 km data set of percent tree cover derived from remote sensing. *Glob. Change Biol.* **6**, 247–254 (2000).
48. Kaplan, J. O. *et al.* Climate change and Arctic ecosystems: 2. Modeling, paleodata-model comparisons, and future projections. *J. Geophys. Res.* **108**, 8171 (2003).
49. McEvedy, C. & Jones, R. *Atlas of World Population History* (Harmondsworth, New York, 1978).
50. Ruddiman, W. F. *Plows, Plagues and Petroleum: How Humans Took Control of Climate* (Princeton Univ. Press, Princeton, 2005).
51. Denevan, W. M. *The Native Population of the Americas in 1492* (Univ. of Wisconsin Press, Madison, 1992).

Supplementary Information accompanies the paper at www.nature.com/naturegeoscience.

Acknowledgements

This article is a contribution to the Global Palaeofire Working Group (GPWG) of the International Geosphere-Biosphere Project Cross-Project Initiative on Fire. The GPWG is supported by the UK Natural Environment Research Council's QUEST (Quantifying Uncertainty in the Earth System) programme. Data compilation and analysis were supported by the QUEST-Deglaciation project (M.J.P., S.P.H.) and by the US National Science Foundation Paleoclimatology (P.J.B.) and Geography and Regional Science programs (P.J.B. and J.R.M.). We thank our colleagues who have made these analyses possible through their contributions to the International Multiproxy Paleofire Database and the Global Charcoal Database.

Author contributions

S.P.H. proposed the idea of a 2000 year synthesis. J.R.M, M.J.P., P.J.B., F.J. and S.P.H. compiled the data. P.J.B. carried out the analyses with assistance from P.E.H., D.G.G. and J.R.M. All authors contributed to writing the paper.

Author information

Reprints and permission information is available online at http://npg.nature.com/reprintsandpermissions. Correspondence and requests for materials should be addressed to J.R.M.

Supplementary Information: Climate and human influences on global biomass burning over the past two millennia

J.R. Marlon, P.J. Bartlein, C. Carcaillet, D.G. Gavin, S.P. Harrison, P.E. Higuera, F. Joos, M.J. Power, I.C. Prentice

The following supplementary material includes 1) information about data sources, including a list of the additional 36 charcoal records included in GCD v.2 and methodological details about our assessment of data coverage in climate and vegetation space; 2) details about the age controls and chronological precision of the records in the database; 3) an evaluation of potential factors affecting charcoal influx variations; 4) details about the reconstructed and simulated climate datasets used in the comparisons; 5) statistical correlation of charcoal and climate series; and 6) the global, zonal, and regional biomass burning reconstructions for regions with sufficient sites along with associated statistics for each composite record.

Data Sources

We obtained 370 sedimentary charcoal records covering part or all of the last two millennia from the Global Charcoal Database (GCD version 1)[51]. The GCD contains charcoal records from different types of sites; we excluded records from marine sediments, which have unknown charcoal source regions, and alluvial fans and soils because these typically have poor temporal resolution and may reflect extremely local fires and not general biomass burning level. We also excluded charcoal records from archaeological sites because these typically reflect fuelwood use as opposed to fires in the surrounding landscape. To improve the regional coverage, an additional 36 sites (Table S1) were obtained from members of the Global Palaeofire Working Group or digitized from the published literature and have been incorporated into a new version of the GCD (GCD version 2).

Number	Site ID	Site Name	Latitude	Longitude
1	417	Artxilondo	43.03	-1.14
2	418	Neublans	46.92	5.34
3	419	Chavannes	46.84	2.37
4	420	Pla de l'Orri	42.50	1.89
5	421	Cuguron	43.10	0.54
6	422	Peyre	44.99	2.72
7	483	Supulah Hill	-4.07	138.58
8	484	Wanda	-2.33	121.23
9	554	Canal de la Puntilla	-40.95	-72.90
10	597	Allom Lake	-25.23	153.17
11	598	Lake Sibaya	-27.21	32.37
12	600	Funduzi	-22.86	30.89
13	610	Lake Teletskoye	25.23	87.65
14	611	Griblje Marsh	45.57	15.28
15	615	Mlaka	45.50	15.21
16	616	El Tiro Bog	-3.84	-79.15
17	621	Boa-1	19.07	-71.03
18	622	Laguna Azul	-52.12	-69.52
19	623	Crevice Lake	45.00	110.58
20	624	Les Comailles	47.66	3.22
21	672	Mizorogaike	35.06	135.77
22	673	Jagaike	35.24	135.46

23	674	Hatchodaira	35.23	135.83
24	676	Ofuke	38.65	135.18
25	682	Bolshoe bog	51.47	104.50
26	683	Duliha bog	51.52	105.00
27	684	Cheremushuka bog	52.75	108.08
28	685	Duguldzeiri River bog	54.45	109.53
29	686	Tompuda bog	55.13	109.77
30	699	Maralay Alas	63.10	130.58
31	700	Sugun Lake	62.08	129.48
32	701	Chai-ku Lake	62.00	130.07
33	712	Lake Lucerne	47.05	8.59
34	713	Bereket Basin	37.55	30.30
35	714	Lago di Pergusa	37.52	14.30
36	716	Xishuangbannan	21.50	101.50

Table S1. Additional charcoal records used in the study with their GCD record locator (Site #). These data are available in GCD version 2:
http://www.bridge.bris.ac.uk/projects/QUEST_IGBP_Global_Palaeofire_WG.

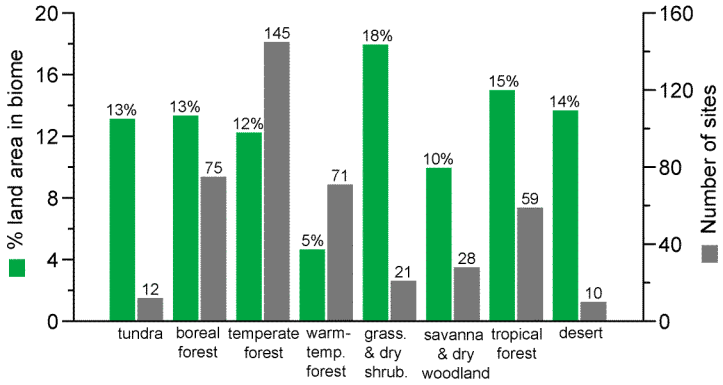

Fig. S1. Percentage of non ice-covered land area in each biome, and proportion of charcoal sites in each biome.

The distribution of charcoal sites was assessed in terms of climate and vegetation and was found to be reasonably representative of all major climatic zones and forest biomes (Fig. 3, main text). The climate at each sampling site and at each point on a global 0.5-degree grid, expressed in terms of growing-season warmth (growing degree days, GDD0, the accumulated temperature sum above 0ºC) and plant-available moisture (the ratio of actual evapotranspiration to equilibrium evapotranspiration), was estimated from a climatology for 1961-1990 (CRU CL 2.0)[52] using algorithms embedded in the BIOME4 global equilibrium terrestrial biogeography-biogeochemistry model[53] and soil properties. We used the model-simulated biome at each site (CLIMATE 2.1) from BIOME4, which has been extensively tested and shown to produce a good simulation of vegetation distribution globally, to represent the natural vegetation cover. The 27 biomes distinguished by the model were grouped into broader units[54]. Estimates of percentage tree cover on the 0.5-degree grid based on remotely-sensed data[55] provided an alternative, independent representation of the actual vegetation cover.

Age Control and Chronological Precision of Charcoal Records

Records in the GCD have age models in calendar years, based on calibration of the original radiocarbon dates at each site using the Fairbanks et al. (2005)[56] calibration program (http://radiocarbon.Ideo.columbia.edu/research/radcarbcal.htm) and a standardized protocol for deriving the best-fit age model. The same procedure was adopted for the 31 new sites added to our data set. Specifically, (a) the core top was considered modern unless the original authors indicated that the surface was disturbed, (b) modern was assumed to correspond to an age of -50 cal yr BP (2000 AD) except in cases where the original publications specifically assigned a date (usually 0 cal yr BP, or 1950 A.D.). Age models were constructed using all available ages, including dated tephra layers and pollen stratigraphic ages, and were based on four possible age model styles: (1) linear interpolation, (2) a polynomial constrained to pass through zero, (3) an unconstrained polynomial fit, and (4) a cubic smoothing spline. The "best fit" age model was selected for each record, based on goodness-of-fit statistics and the appearance of the resulting curve (i.e., ensuring that new models did not introduce age reversals)[51].

Data Standardization and Normalization

We used the following procedure to limit the influence of sedimentation rate changes on the composite charcoal records (see Evaluation of Potential Factors Influencing Charcoal Influx Variations below), and to ensure comparability among a broad range of data types and charcoal quantification methods:

(1) All non-influx data (e.g., concentration expressed as particles/cm^3/yr; charcoal-to-pollen ratios) were converted to influx values (i.e. particles/cm^2/yr) or quantities proportional to influx, by dividing the charcoal values by sample deposition times (yr/cm).
(2) The variance of individual records was homogenized using the Box-Cox transformation:

$$c_i^* = \begin{cases} ((c_i' + \alpha)^\lambda - 1)/\lambda & \lambda \neq 0 \\ \log(c_i' + \alpha) & \lambda = 0 \end{cases}$$

where c_i^* is the transformed value, λ is the Box-Cox transformation parameter and α is a small positive constant (here, 0.01) added to avoid problems when c_i' and λ are both zero. The transformation parameter λ was estimated by using a maximum likelihood procedure[57], and was based on all charcoal values in each record spanning the past 2050 years.
(3) Because the Box-Cox transformation results in values that are comparable only among data sets with identical λ values, the transformed data were rescaled to the range (0, 1) using the minimax transformation:

$$c_i' = (c_i - c_{\min})/(c_{\max} - c_{\min})$$

where c_i' is the transformed value of the *i*-th sample in the record and c_i, and $c_{\max}$ and $c_{\min}$ are the maximum and minimum values over the past 2050 years.

(4) The transformed and rescaled values were converted to Z-scores by subtracting the mean value and dividing by the standard deviation of the past 2050 years, to express the data as anomaly values, or differences from a long-term average.

Data Smoothing and Construction of the Composite Records

To construct the global and regional composite charcoal records, we tested several alternative processes (fig. S2) and adopted a two-stage smoothing method. Individual records were "pre-smoothed" to ensure that records with unusually high sample resolution (e.g. Crawford Lake[58]) did not have a disproportionate influence in the composite record. Smoothing was performed using locally weighted regression, or "lowess"[59]. The lowess approach minimizes the influence of outliers, which helps filter noise from the charcoal data. In implementing lowess, we used a constant window width and fixed target points (in time), as opposed to a constant proportion or span of data points and fitting at each data point[60]. The lowess function used the customary tricube

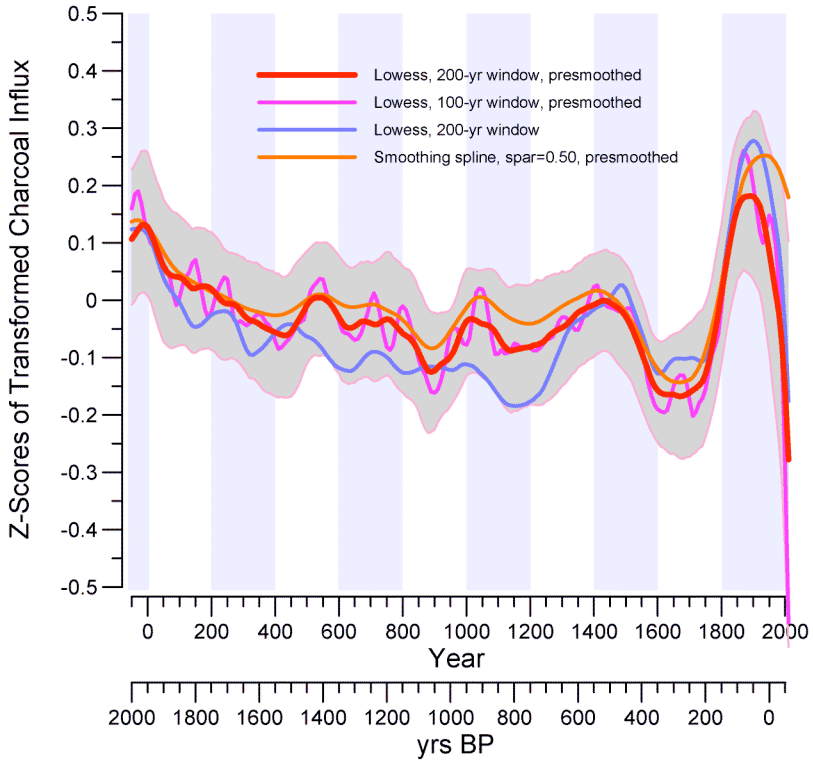

Figure S2. Alternative (global) composite curves, including fitted values determined using the presmoothed values and a 200-yr window (red), the presmoothed values and a 100-yr window (purple), the transformed and rescaled individual charcoal values (blue), and the fitted values from the application of a smoothing spline with a 0.50 smoothing parameter (orange).

weight function, a first-degree or linear fit at each target point, and a single "robustness iteration." The presmoothing window width was 20 years, with a fit of order 0 (i.e., a locally weighted mean) and a robustness parameter of 0, thus including all data values that fall within the window when calculating the local mean. A single value was thus produced for each non-overlapping 20-year interval from 50 BC to 2000 AD, ensuring that the value for each 20-year window was based on all samples (for records with high

temporal resolution) and also that data were not interpolated within low-resolution segments of records or extrapolated into missing segments of records. The lowess technique was also used to create the composite charcoal curves (Fig. 1A), based on a 200-yr window that emphasizes centennial-scale variations in the charcoal data. The smooth curves shown here are constructed by determining fitted values at 10-year intervals. (Window-widths here refer to the full span of the window, not the half-width).

Confidence intervals for the global and regional composites were generated by a bootstrap approach in which individual sites (not samples) were sampled with replacement over 1000 replications. The approach allows us to asses the sensitivity of the results to the inclusion or exclusion of individual sites. Bootstrap confidence intervals for each target point were the 2.5th and 97.5th percentiles of the fitted values for that target point. The number of samples, age control, and spatial distribution of records contributing to each summary series is illustrated in figures S6-S15.

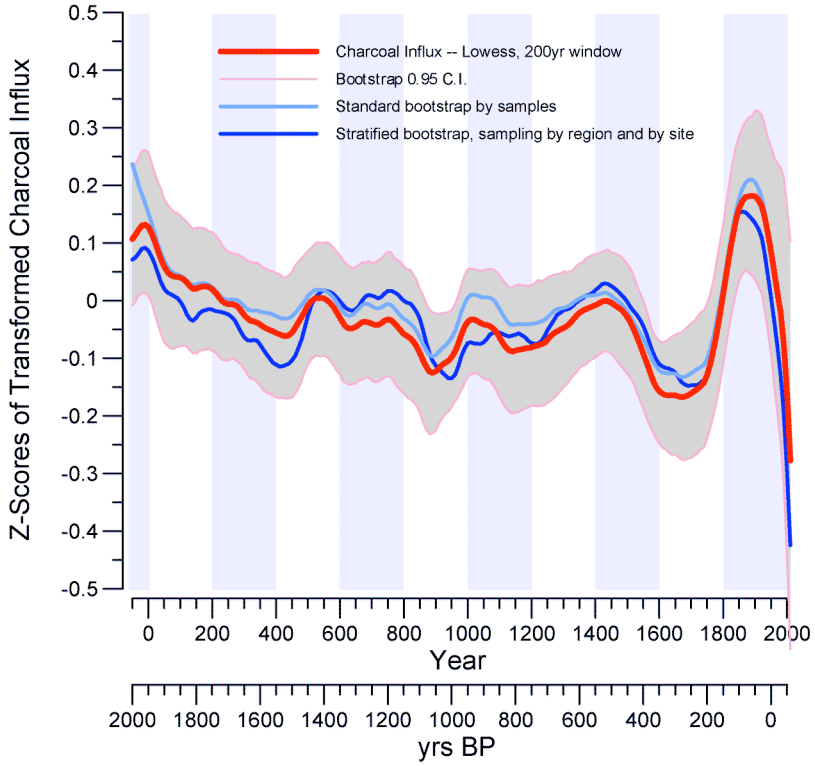

Figure S3. Evaluation of the impact of site distribution on the composite records.

We also assessed the degree to which the global composite record was influenced by the uneven spatial distribution of sites by examining alternative bootstrap approaches. We considered (1) sampling with replacement of individual samples (the conventional approach), (2) sampling with replacement of individual sites (the approach used here), and (3) stratified resampling based on sampling pre-defined regions (with replacement) and then sampling (with replacement) sites within the selected region (which upweights the influence of regions represented by fewer sites). The resulting curves (fig. S3) fall within the confidence limits on our standard curve, have a similar temporal structure, and

identify the same century-scale local maxima. This strongly suggests that the global summary curve is not appreciably influenced by the uneven distribution of sites among regions. In addition, we examined the relationship between the global composite records and potential factors affecting charcoal influx variations, such as sedimentation rates (fig. S4) and found the composite to be robust to such influences.

Evaluation of Potential Factors Affecting Charcoal Influx Variations

In paleofire research in general, the possibility of changing sedimentation rates in lake cores motivates the examination of charcoal influx, as opposed to charcoal concentrations. However, the remarkable charcoal influx variations in the last few centuries warranted an examination of the effects of using charcoal concentration as opposed to influx, of varying sedimentation rates, and possible uncertainties in age model construction on the composite curves. Sedimentation rates are artificially high near the top of lake-sediment cores because of the high water content and possibly higher erosion rates after land-cover changes, and thus we evaluated the possibility that features observed in the charcoal curve in Fig. 1 (main text) were artifacts of these processes.

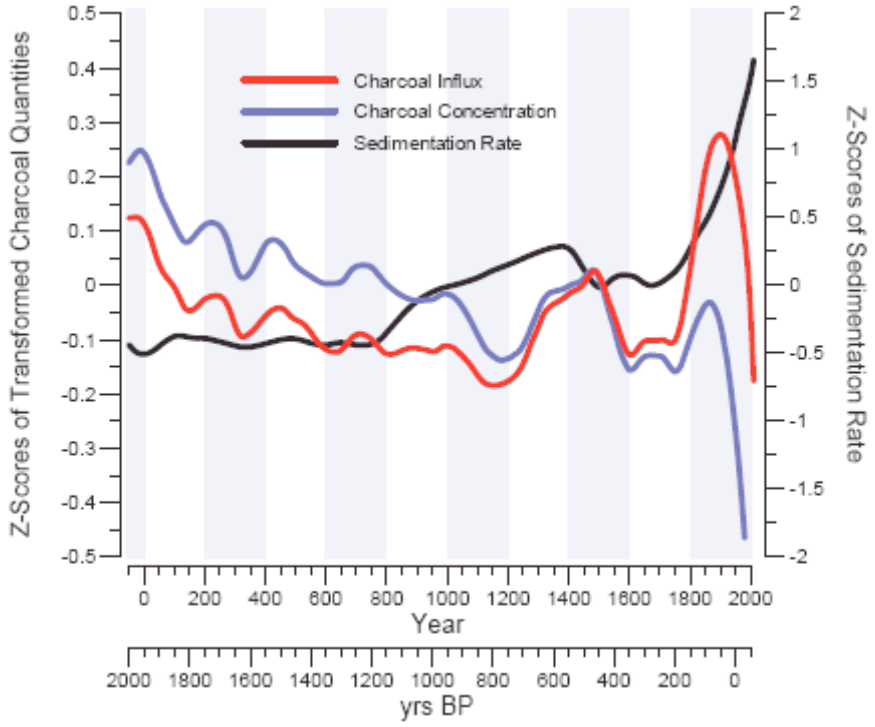

Fig. S4. Smoothed values of charcoal concentration, influx, and sedimentation rate. The concentration, influx, and sediment rate of individual samples were summarized by curves constructed by locally weighted regressions (i.e. "lowess curves") using a constant window width of 200 years, the tricube weight function, and one "robustness iteration."

A simple model was created to assess the impact of changing sedimentation rates and down-core sediment dewatering on charcoal concentration and influx data (P.J. Bartlein and D.G. Gavin, unpublished results). Figure S4 shows composite curves across sites based on charcoal concentration, influx, and individual-sample sediment rates (all

smoothed the same way as the charcoal influx data in Fig. 1, main text). Sedimentation rates show the expected increase over time, while charcoal concentration and influx show the characteristic upturn around 1750 A.D. and downturn after 1850 A.D. The only way the model can generate features similar to those observed in the influx data is by manipulating sedimentation rate or concentration in unrealistic ways.

Comparison of concentration data, influx data, and sedimentation rates (Fig. S4) shows that the long-term trend in the concentration data inversely reflects the long-term trend in sedimentation rate, which increases towards present. The distinct downward trend in the influx data cannot be accounted for by changes in sedimentation rate. Centennial-scale variability in both concentration and influx shows no consistent relationship with changes in sedimentation rate. The peak in charcoal concentration and influx at ca. 1850 A.D. (Figure 1, main text, Fig. S4) is coincident with a steady increase in sedimentation rate and is therefore not an artifact due to changes in sedimentation rates.

The variations in charcoal accumulation are thus highly robust to differences in pre-treatment methods. However, additional factors increase the uncertainty of the composite reconstructions for recent decades, including the assignment of an age for the "modern" core top (i.e. 1950 A.D. or 2000 A.D.), the use of a different method (Pb210 versus 14C) to date recent decades, the high water content of surface samples, and potentially large changes in erosion and sediment disturbance due to human activities. To highlight the increased uncertainty in our reconstructions in recent decades, changes in biomass burning post-1950 are shown as a dashed line. Other sources of data, e.g. forestry records, fire-scar or tree-ring records, or remote-sensing, are likely to provide more accurate tools for reconstructing changes in fire regimes than sedimentary records over this period53.

Comparison with NCAR climate simulations

Climate-model simulations provide an alternative realization of long-term climate changes. We have compared the composite charcoal record to results from a 1000-year simulation[61] with the National Center for Atmospheric Research Climate System Model (NCAR CSM), Version 1.4, a global coupled atmosphere-ocean-sea ice-land surface model without flux adjustments[62, 63]. The NCAR CSM1.4 model was forced over the period from 850 to 2000 A.D. using observation-based records of solar irradiance, spatially explicit aerosol loading from explosive volcanism, the greenhouse gases CO2, CH4, N2O, CFC-11 and CFC-12, and anthropogenic sulfate aerosols, plus a recurring annual cycle of ozone and natural sulfate aerosol. Other forcing factors, such as orbital parameter changes (very slow forcing, constant 1400 A.D. conditions were used) and vegetation/land use changes (highly regional in impact), were not included. The solar irradiance history over the past 1150 years was based on a recent 10Be history and solar irradiance was scaled to a reduction during the Maunder Minimum (1645-1715 A.D.) of 0.25% relative to present[64]. The volcanic forcing was established by converting ice-core aerosol proxies to latitudinal and temporally varying atmospheric aerosol fields. Atmospheric CO2, CH4 and N2O concentrations were individually prescribed based on ice-core measurements and direct atmospheric observations. The CFC-11, scaled to take

into account the radiative forcing by other halocarbons and SF6[65], and CFC-12 concentration histories are based on historic emission data and recent measurements. The results are given as detrended residuals after subtracting a millennial-scale spline fit for individual months of the annual cycle at each model grid point obtained from a control integration. Further details of these simulations (model setup and simulated climate) are available elsewhere[61].

We compared the composite global fire reconstruction for the past 1000 years with simulated global temperature and precipitation from the NCAR CSM1.4 simulation. There is broad similarity between the simulated temperature record and the charcoal-based fire record (Fig. S5) over much of this interval. However, in general the simulated changes are smoother than those shown in the global fire reconstruction and the feature corresponding to the "Little Ice Age" interval in the fire reconstruction is more distinct. The marked upward trend in fire activity after ca 1750 A.D. corresponds to a marked upward trend in the simulated temperature curve, supporting our suggestion that climate change could have contributed to the observed increase in fire. The most striking disparity between the two records is post-1950 when charcoal decreases while climate continues to warm. This difference supports our suggestion that this feature of the composite global fire reconstruction is driven by direct human action rather than by climate. There is no clear relationship between the composite global fire reconstruction and simulated precipitation changes. This suggests that the principal climatic driver for changes in biomass burning at a global scale is changes in temperature, rather than precipitation.

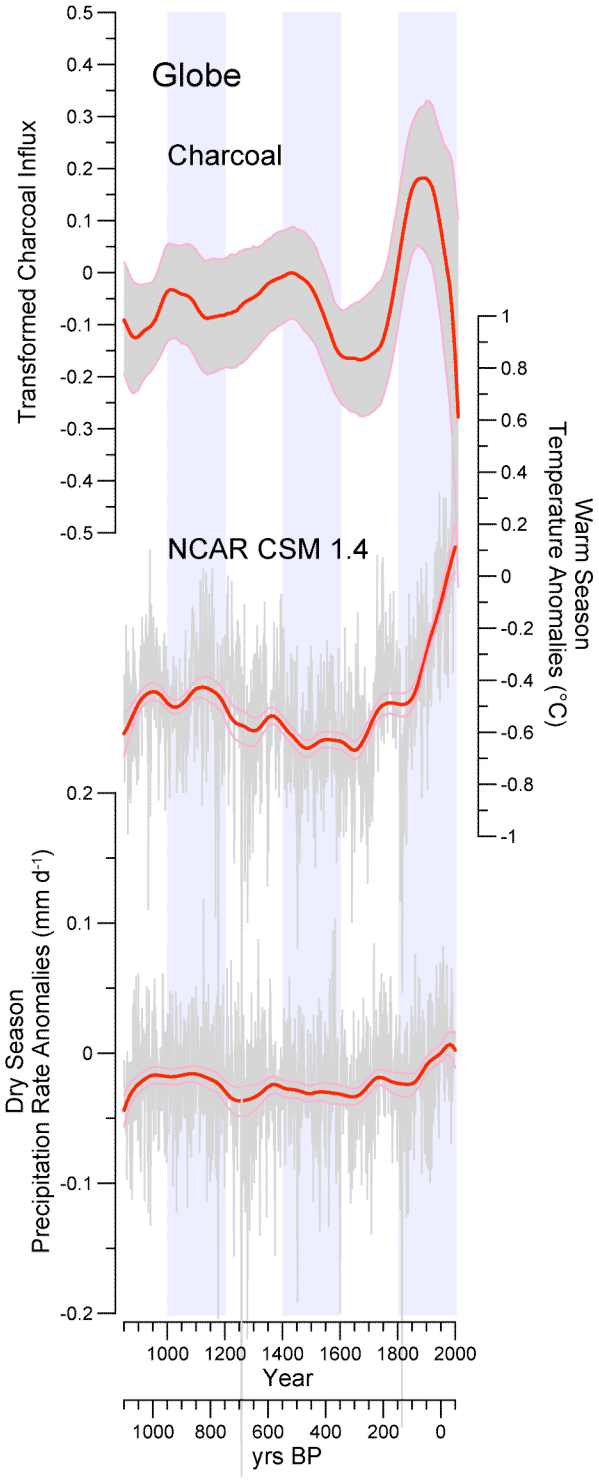

Fig. S5. (a) Reconstruction of global biomass burning, with NCAR CSM1.4 simulated (b) warm season temperature anomalies, and (c) dry season precipitation rate anomalies. Simulated data are for land only and are also shown smoothed and with 95% confidence intervals in the same manner as the charcoal records.

Correlation of Charcoal and Climate Time Series (1-1750 A.D.)

Quantitative assessment of the significance of the correlation between the charcoal and climate curves shown in Fig. 1 is difficult because the individual series are each autocorrelated, which arises both from the long-term trend in both series and from the way in which the summary series were created. A simple linear regression between the bidecadal "presmoothed" standardized charcoal influx values, and similarly averaged reconstructed Northern Hemisphere temperature values is significant,

$$z_t = 0.07 + 0.27T_t + a_t;\ F = 4.46;\ p < 0.05;\ s^2 = 0.012;\ AIC = -130.49;$$

where z_t is the smoothed transformed and standardized charcoal influx in year t, and T_t is the average reconstructed temperature in year t. However, the residuals, a_t, from this regression are cross-correlated at several lags with the temperature time series, and are also weakly autocorrelated. A relatively simple model that links charcoal and reconstructed climate is an IMA(1,1) model for charcoal, with temperature as an exogenous predictor:

$$z_t = -0.83 + z_{t-1} + 0.07T_t + a_t;\ s^2 = 0.011;\ AIC = -136.06.$$

This model fits the data slightly better, and produces residuals that are not autocorrelated or cross-correlated with temperature (as measured using the Box-Ljung test)

Global, Zonal, and Regional Biomass Burning Reconstructions and Associated Statistics

The global composite reconstruction of biomass burning (Fig. S6b) is based on transformed, rescaled, and standardized charcoal values (Fig. S6a). Although the number of sites contributing to the global curve varies through time, there are never less than 80 sites comprising the average for each time interval (Fig. S6c). Most records in the global composite have a sampling resolution greater than one sample per 50 years, and many have a resolution of one sample per 10-20 years (Fig. S6f). There is reasonable dating control throughout the period of interest and only five of the 20-year time windows lack radiometric dates (Fig. S6d). These analyses suggest that the variations in the global composite are unlikely to be artifacts related to sample density.

The robustness of the zonal reconstructions of fire history (Fig. 2, main text) can be assessed on the basis of figures S8 to S11. As might be expected given the land area within each zone (Fig. 2, main text), the number of sites contributing to the reconstruction, sampling density, and age control are all higher for the northern hemisphere extratropics than for other zonal reconstructions. Nevertheless, there are more than 10 sites contributing to all zonal reconstructions in nearly every time interval, and the sampling resolution and dating control are sufficient to ensure confidence in the reconstruction of long-term trends and centennial-scale variability. These reconstructions are discussed in the main text.

We examined composite records of fire history for a number of regions, defining regions on the basis of broad-scale atmospheric-circulation controls on modern and past climate regimes. Some regions have too few sites to provide a coherent picture of regional changes. Here, we present results for regions with more than 10 sites contributing to most 20-year windows during at least the past 1000 years (Figs. S12-S16). The sample size per 20-year interval and the proportion of global ice-free land area are also shown.

The regional composites show that the initial long-term downward trend characteristic of the global composite fire history is expressed in western North America (Fig. S11), Asia (Fig. S14) and Central and tropical South America (Fig. S15). The trend is weak in the composite records for eastern North America (Fig. S12) and Europe (Fig. S13). The records from Asia (Fig. S14), like the zonal records of the tropics (Fig. S8) and southern extratropics (Fig. S9), suggest variable levels of biomass burning prior to ca 1800 AD. With the exception of Central and tropical South America (Fig. S15), all regions display a marked upturn in the second half of the 19th century, although the timing of this increase varies. The marked downturn during the first half of the 20th century is clear in the regional composite records from western North America (Fig. S11), Asia (Fig. S14), and Central and tropical South America (Fig. S15). Although there is a wealth of information in these regional fire history records, analyzing these patterns and their relationships with regional climate, population and land-use changes, is beyond the scope of this paper.

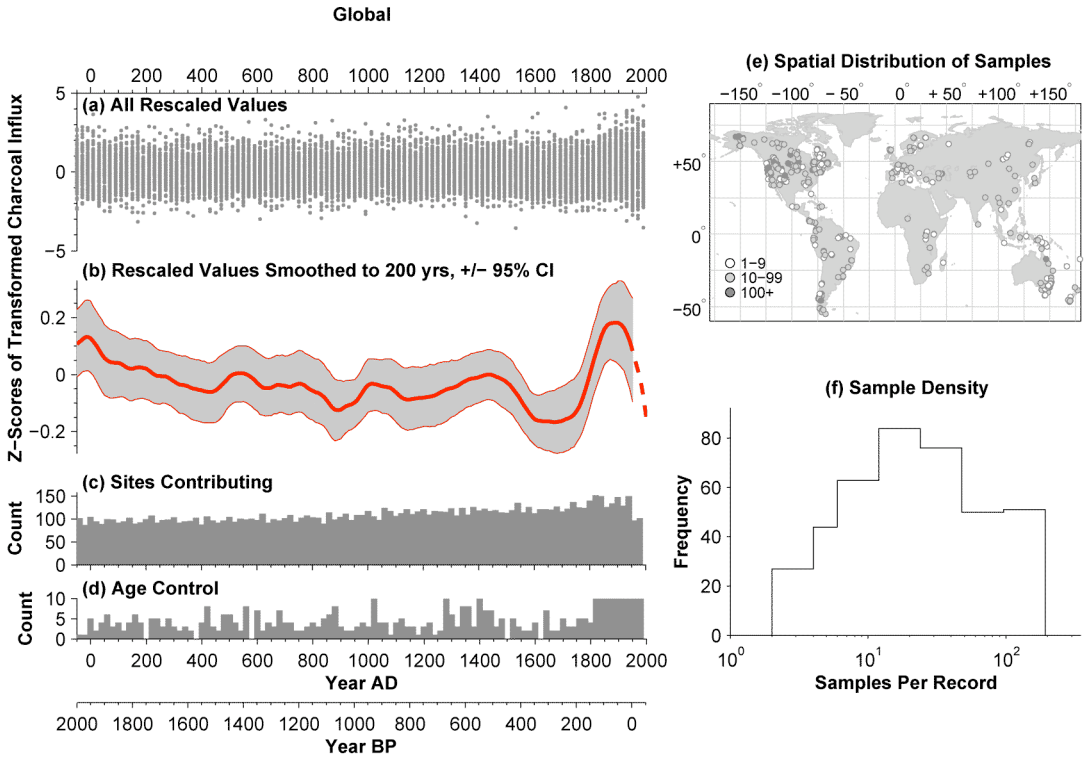

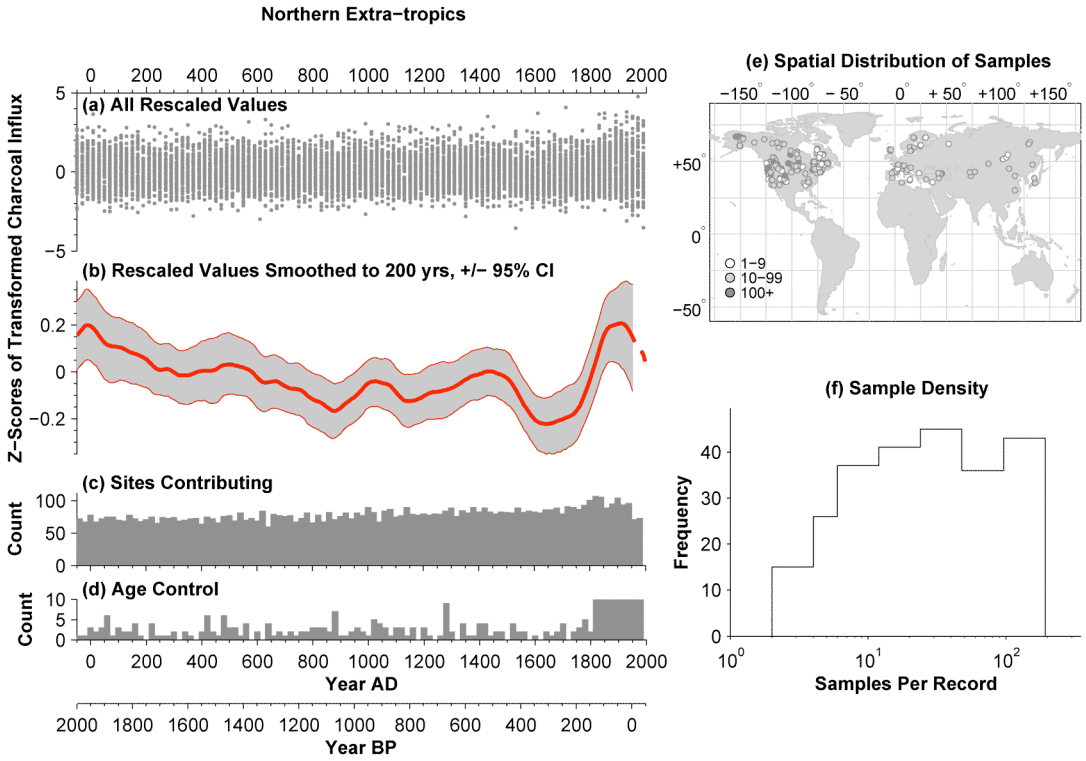

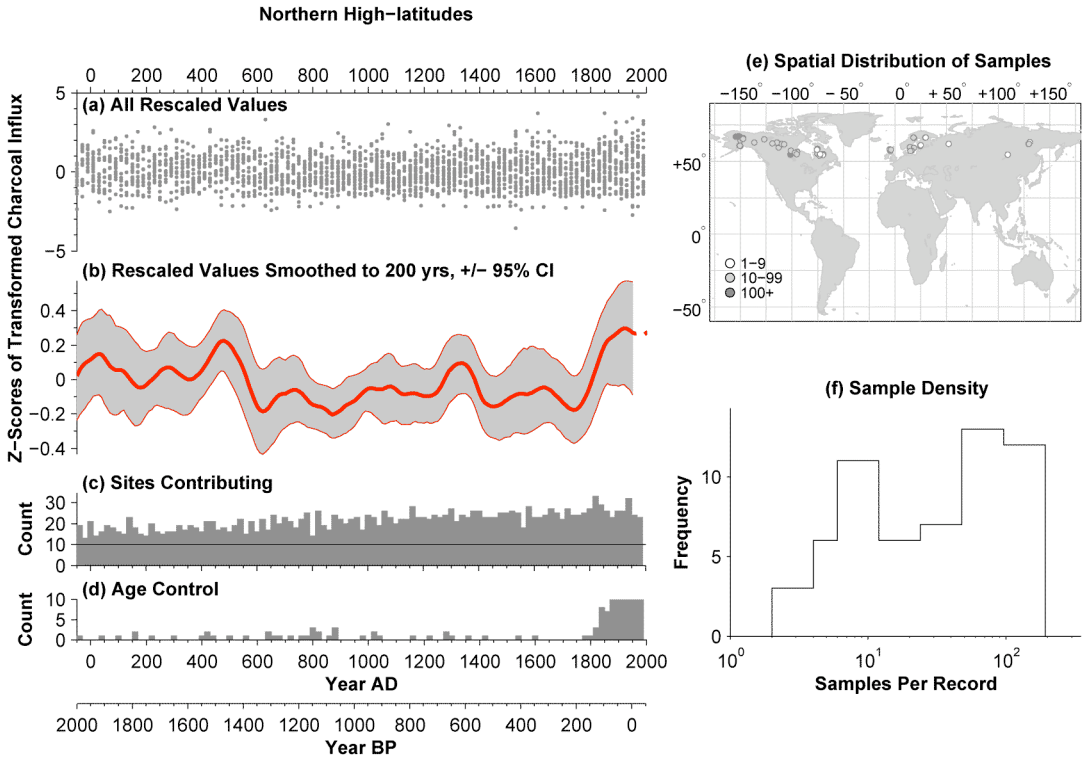

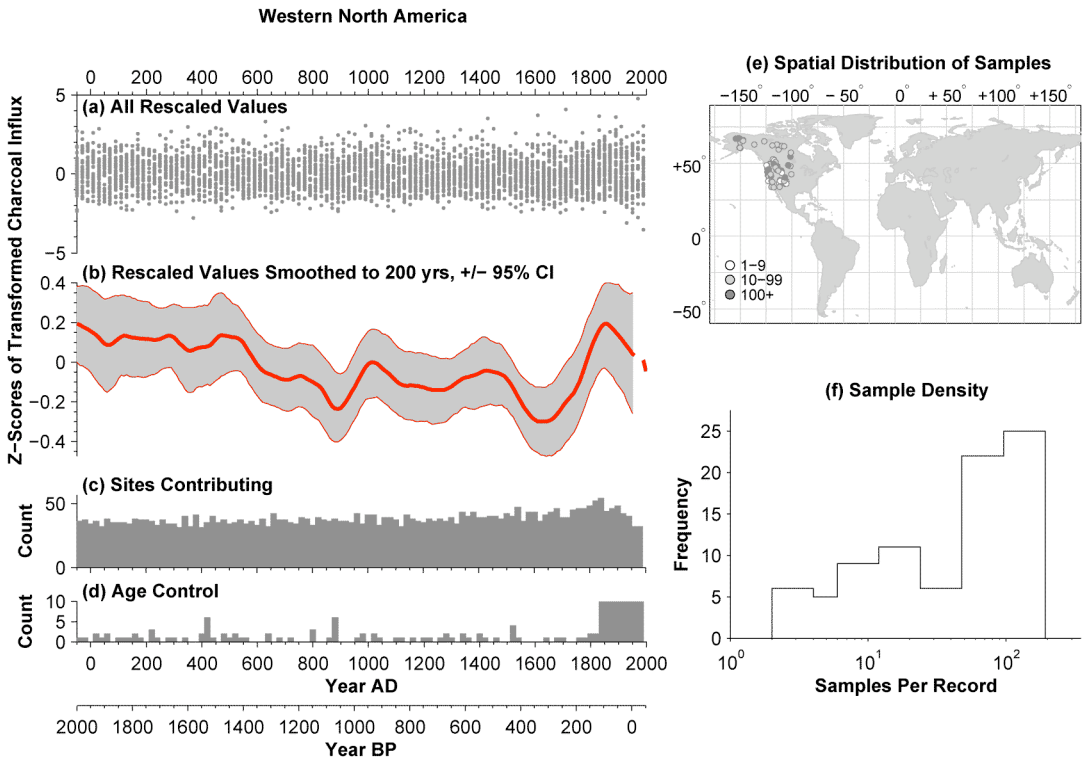

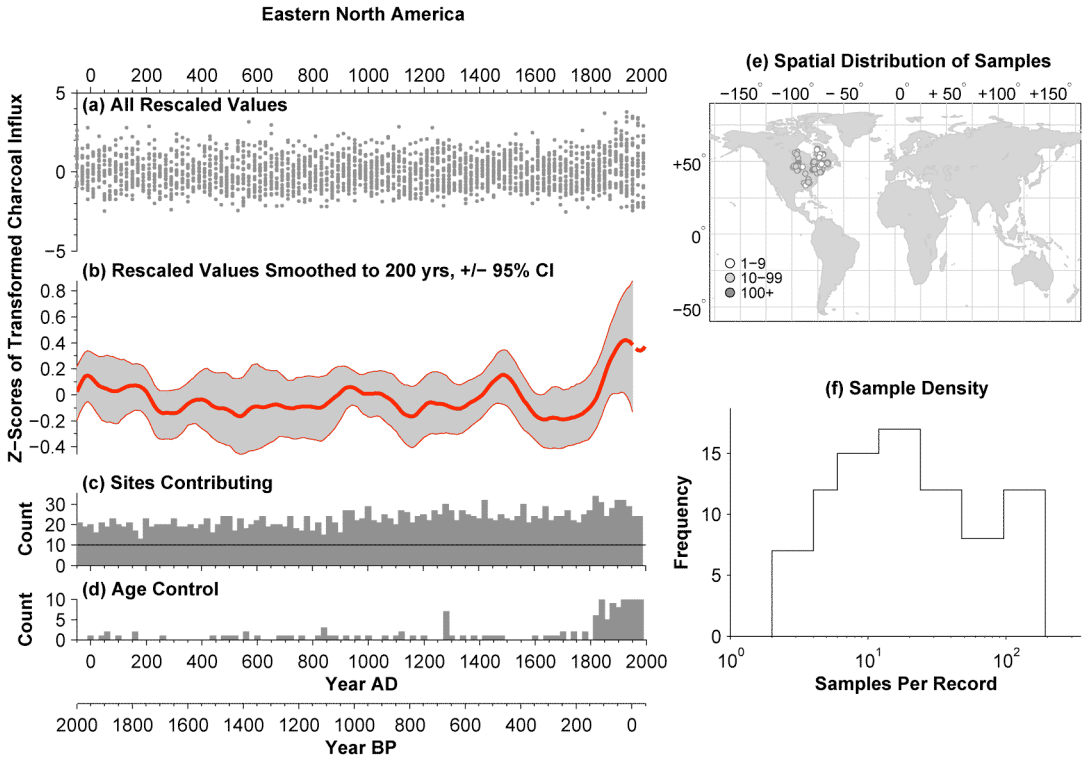

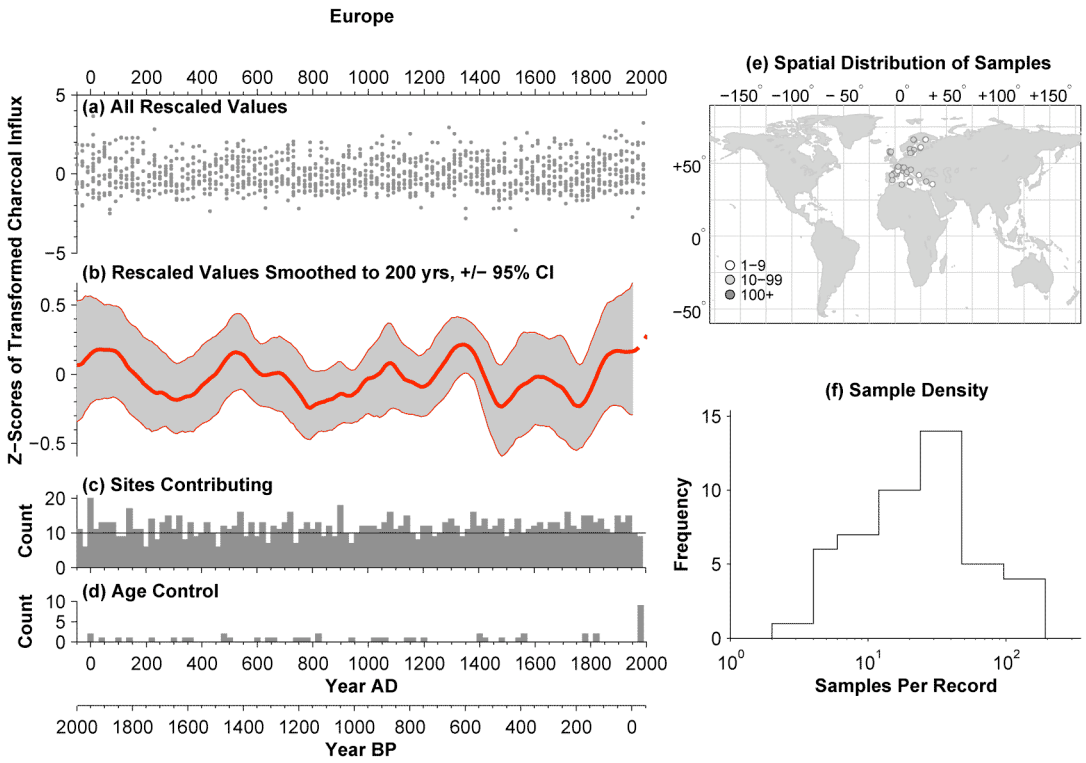

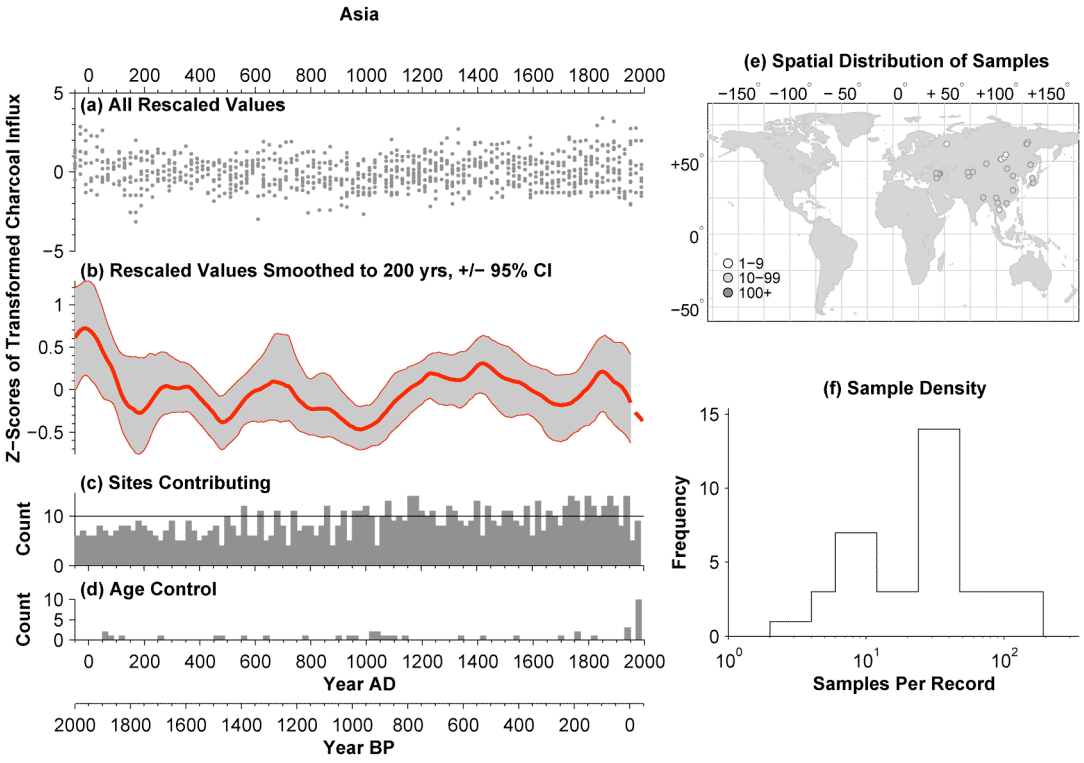

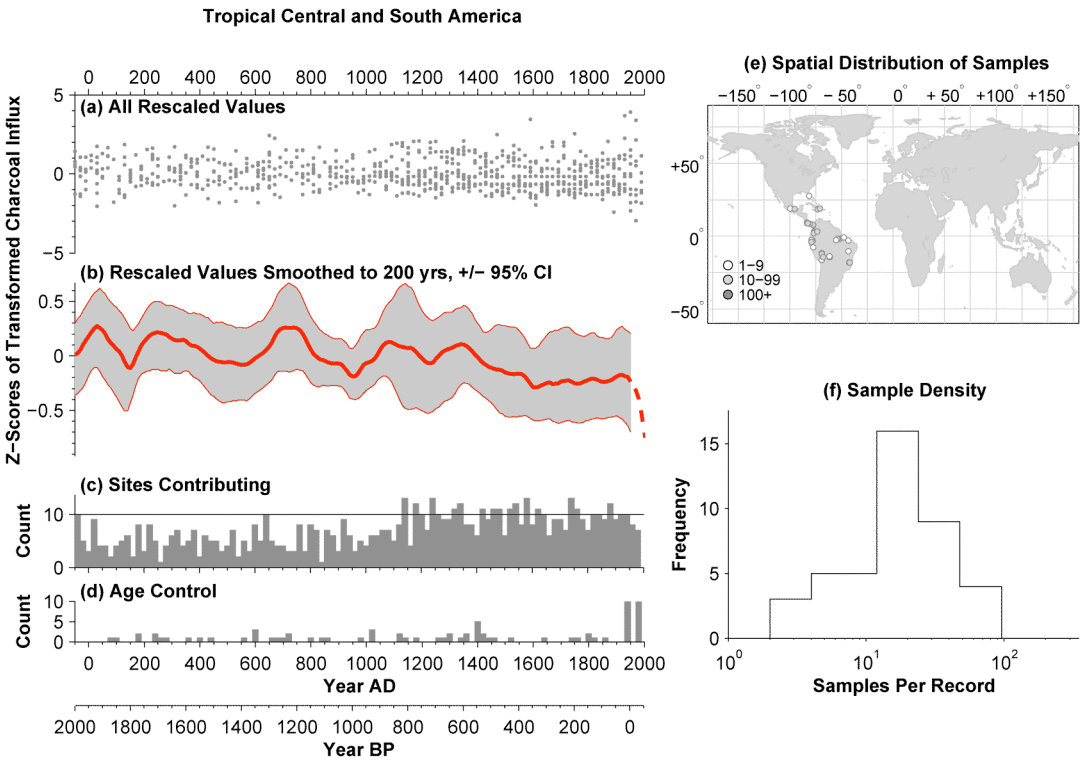

Figs. S6 – S15: (a) Rescaled and transformed charcoal influx values on equal 20-year intervals. (b) Composite charcoal curve with confidence intervals. (c) Number of sites contributing at least one sample to each 20-year interval in the composite record. (d) Number of 14C or 210Pb dates contributing to chronological control for each 20-year interval in the composite record. (e) Spatial distribution of sites contributing to the composite record, with the number of samples at each site reflected by the shade of each dot. (f) Histogram of sample density within each individual record contributing to the composite record. Note the log scale on the x-axis.

References for Supplementary Information

51. Power, M. J. *et al.* Changes in fire regimes since the Last Glacial Maximum: an assessment based on a global synthesis and analysis of charcoal data. *Clim. Dynam.* **30**, 887-907 (2007).
52. New, M., Lister, D., Hulme, M. & Makin, I. A high-resolution data set of surface climate over global land areas. *Clim. Res.* **21**, 1-25 (2002).
53. Kaplan, J. O. *et al.* Climate change and Arctic ecosystems: 2. Modeling, paleodata-model comparisons, and future projections. *J. Geophys. Res.* **108**, 8171 (2003).
54. Harrison, S. P. & Prentice, C. I. Climate and CO2 controls on global vegetation distribution at the last glacial maximum: analysis based on palaeovegetation data, biome modelling and palaeoclimate simulations. *Glob. Change Biol.* **9**, 983-1004 (2003).
55. DeFries, R., Hansen, M., Townshend, J. R. G., Janetos, A. C. & Loveland, T. R. A new global 1km data set of percent tree cover derived from remote sensing. *Glob. Change Biol.* **6**, 247-254 (2000).
56. Fairbanks, R. G. *et al.* Marine radiocarbon calibration curve spanning 0 to 50,000 years B.P. based on paired 230Th/234U/238U and 14C dates on pristine corals. *Quat. Sci. Rev.* **24**, 1781–1796 (2005).
57. Venables, W. N. & Ripley, B. D. *Modern applied statistics with S* (Springer Verlag, New York, 2002).
58. Clark, J. S. & Royall, P. D. Local and regional sediment charcoal evidence for fire regimes in presettlement north-eastern North America. *J. Ecol.* **84**, 365-382 (1996).
59. Cleveland, W. S. & Devlin, S. J. Locally weighted regression: an approach to regression analysis by local fitting. *J. Am. Stat. Assoc.* **83**, 596-610 (1988).
60. Jacoby, W. G. *Statistical graphics for univariate and bivariate data* (Sage Publications, Thousand Oaks, Calif., 1997).
61. Ammann, C. M., Joos, F., Schimel, D. S., Otto-Bliesner, B. L. & Tomas, R. A. Solar influence on climate during the past millennium: Results from transient simulations with the NCAR Climate System Model. *Proc. Natl. Acad. Sci. USA* **104**, 3713-3718 (2007).
62. Boville, B. A., Kiehl, J. T., Rasch, P. J. & Bryan, F. O. Improvements to the NCAR CSM-1 for transient climate simulations. *J. Clim.* **14**, 164-179 (2001).
63. Otto-Bliesner, B. L. & Brady, E. C. Tropical Pacific variability in the NCAR Climate System Model. *J. Clim.* **14**, 3587-3607 (2001).
64. Lean, J., Beer, J. & Bradley, R. Reconstruction of solar irradiance since 1610: implications for climate change. *Geophys. Res. Lett.* **22**, 3195-3198 (1995).
65. Joos, F. *et al.* Global warming feedbacks on terrestrial carbon uptake under the Intergovernmental Panel on Climate Change (IPCC) emission scenarios. *Glob. Biogeochem. Cycles* **15**, 891-907 (2001).